Magnetic inelastic dark matter: Directional signals without a directional detector

Magnetic Inelastic Dark Matter: Directional Signals Without a Directional Detector

Tongyan Lin[1] and Douglas P. Finkbeiner[1,2]

[1]*Physics Department, Harvard University, Cambridge, MA 02138, USA*
[2]*Harvard-Smithsonian Center for Astrophysics, 60 Garden St., Cambridge, MA 02138, USA*

(Dated: July 26, 2013)

The magnetic inelastic dark matter (MiDM) model, in which dark matter inelastically scatters off nuclei through a magnetic dipole interaction, has previously been shown to reconcile the DAMA/LIBRA annual modulation signal with null results from other experiments. In this work, we explore the unique directional detection signature of MiDM. After the dark matter scatters into its excited state, it decays with a lifetime of order 1 μs and emits a photon with energy $\sim$100 keV. Both the nuclear recoil and the corresponding emitted photon can be detected by studying delayed coincidence events. The recoil track and velocity of the excited state can be reconstructed from the nuclear interaction vertex and the photon event vertex. The angular distribution of the WIMP recoil tracks is sharply peaked and modulates daily. It is therefore possible to observe the directional modulation of WIMP-nucleon scattering without a large-volume gaseous directional detection experiment. Furthermore, current experiments such as XENON100 can immediately measure this directional modulation and constrain the MiDM parameter space with an exposure of a few thousand kg $\cdot$ day.

PACS numbers: 95.35.+d

I. INTRODUCTION

Despite decades of direct detection efforts [1], the nature of dark matter interactions with regular matter remains elusive. The results from the DAMA/NaI and DAMA/LIBRA collaborations suggest that such interactions may be more intricate than originally expected. DAMA has observed an annual modulation in NaI crystals for the past decade [2–4], with the expected phase for WIMP-nuclei interactions. There is no experimental evidence corroborating this signal. By now, it appears that the signal is not conventional spin-independent elastic scattering of WIMPs on nuclei.

Among the quantitative explanations of DAMA, it is possible to take a few approaches. One method is to exploit detector effects, such as channeling [5–7]. Another is to introduce a dark matter model with more ingredients (for example, [8–13]). A possibility is that the dark matter preferentially scatters off the NaI used in DAMA, as opposed to the nuclei used in other direct detection experiments. In particular, we focus on the fact that iodine is special in having both a relatively large mass and a relatively large magnetic moment [14].

If dark matter has (weak) electromagnetic moments [15, 16], it can interact through the charge and magnetic dipole moment of the nuclei. For a summary of the interaction strengths for various nuclei used in direct detection experiments, see [17]. This type of interaction has been used to explain some recent direct detection results [17–22], including the positive claim of DAMA. However, there are strong constraints from CDMS [23] and XENON [24, 25] on this explanation of DAMA.

Inelastic dark matter (iDM) takes advantage of the large iodine mass [26]. In iDM, there is an excited state of dark matter with mass splitting δ. It is assumed that dark matter couplings with nuclei are primarily off-diagonal, so that the WIMP is scattered into its excited state. This interaction only occurs if the dark matter has sufficient initial velocity. The minimum velocity v_{min} for a WIMP to scatter with a nuclear recoil of energy E_R is:

$$v_{min} = \frac{1}{\sqrt{2m_N E_R}}\left(E_R\left(\frac{m_N}{m_\chi}+1\right)+\delta\right) \qquad (1)$$

where m_N is the nucleus mass and m_χ is the WIMP mass. For splittings of $\delta \sim 100$ keV, experiments are only sensitive to the tail of the WIMP velocity distribution, leading to a much larger annual modulation than in the elastic case. Furthermore, scattering on heavier nuclei like iodine is preferred if m_χ is of order 100 GeV.

The basic iDM model is now tightly constrained [27] by the latest results from CRESST [28], ZEPLIN-III [29], XENON [24], and CDMS. It is possible to combine inelastic scattering with yet more ingredients. For example, spin-dependent inelastic scattering is discussed in [30].

A. Magnetic Inelastic Dark Matter

We focus on magnetic inelastic dark matter (MiDM), because it has a unique and interesting directional signature. Chang et al. [14] showed MiDM could explain both DAMA and other null results. The model takes advantage of both the magnetic moment and large mass of iodine. In MiDM, the dark matter couples off-diagonally to the photon:

$$\mathcal{L} \supset \left(\frac{\mu_\chi}{2}\right)\overline{\chi}^*\sigma_{\mu\nu}F^{\mu\nu}\chi + c.c. \qquad (2)$$

where the mass of χ and χ^* are split by $\delta \sim 100$ keV. The off-diagonal coupling is natural if the dark matter is a Majorana fermion. The excited state has a lifetime $\tau = \pi/(\delta^3\mu_\chi^2) \sim 1 - 10\mu$s, and emits a photon when it

m_χ (GeV)	δ (keV)	μ_χ/μ_N	τ (μs)	λ (m)	$\eta_{.15}$	Angular Rate 10^{-3}(cpd/kg)	XENON100 (non-blind)
70*	123	6.2×10^{-3}	1.2	0.4	0.23	11.3	1.4
140*	109	2.2×10^{-3}	12.7	6.2	0.018	2.2	8.1
300*	103	2.0×10^{-3}	18.0	9.7	0.012	1.7	11.6
70	135	11.2×10^{-3}	0.26	0.09	0.63	17.6	0.07
140	125	3.2×10^{-3}	3.9	2.0	0.06	4.4	3.3
300	117	2.5×10^{-3}	7.9	4.4	0.03	2.6	5.8
70	100	2.5×10^{-3}	12.6	4.9	0.024	2.7	9.2
140	90	1.6×10^{-3}	42.2	20.2	0.006	1.3	22.2
300	90	1.6×10^{-3}	42.2	22.1	0.005	1.0	19.3

TABLE I: In the first three (starred) rows, we give the best fit benchmark models of MiDM, with $v_{esc} = 550$ km/s and $v_0 = 220$ km/s [14]. We also list parameters within the 90% CL region of each best fit value, for which the lifetime, τ, can be a factor of a few larger or smaller. λ is the average recoil track length. $\eta_{.15}$ is an estimate of the efficiency of XENON100 to detect delayed coincidence events, as described in Section II B. The 'angular' rate is the rate for delayed coincidence events with a nuclear recoil in the energy range $10 - 80$ keVr, followed by a photon with δ keVee. This is obtained from multiplying the total rate by $\eta_{.15}$. We also show the expected number of nuclear recoil events for the published XENON100 non-blind analysis.

decays. This short lifetime makes it possible to observe both the nuclear recoil and the emitted photon with a meter-scale detector. The two interaction vertices allow reconstruction of the excited state track. Both the velocity and angle can be measured, enabling directional detection even without a directional detector.

A dark matter particle with a permanent electromagnetic dipole moment generally can be constrained by, e.g., gamma-ray measurements, the CMB, or precision Standard Model tests [31–33]. However, the strongest bounds tend to come from direct detection experiments themselves, at least in the 100 GeV mass range. Furthermore, in MiDM, the inelastic nature of the interaction suppresses interactions with photons and baryons at low energies. If the dark matter is a composite particle, a low compositeness scale can also suppress annihilation to photons.

There are some variants of the MiDM idea. In [34], the parameter values were taken to be $m_\chi \sim 1$ GeV and $\delta \sim 3$keV. The DAMA signal is produced by the emitted photon. This explanation evades constraints from other direct detection experiments because such low-energy electromagnetic events are typically rejected or not seen by other detectors.

It is also possible that the dark matter couples to a new 'dark' $U(1)$, with gauge boson mass $m_A \neq 0$ [22, 35, 36]. Here the dark matter has a large dark dipole. If the dark gauge boson couples to regular electromagnetic currents, a sizable interaction with nuclei can be generated. However, the decay rate of the excited state is suppressed because there is no direct interaction with the photon. While these ideas are interesting explanations of the DAMA signals, we do not consider them further because the excited state has a long lifetime.

We study MiDM benchmarks, given in Table I, which are good fits to the DAMA annual modulation signal [14]. MiDM models with m_χ greater than ~ 300 GeV are severely constrained by ZEPLIN-III [29], KIMS [37], and XENON100 [25].

The benchmarks are subject to form factor and velocity distribution uncertainties [38–42], especially for larger masses. The directional signal prediction can change wildly depending on the lifetime and rate.

In order to explore the parameter space, we also considered two extreme points within the DAMA 90% confidence level region found by [14], for each of the three masses. For the point with highest δ and μ_χ, the expectation for directional detection is better. The point with lowest δ and μ_χ, which would not result in many delayed coincidence events, is in any case already tightly constrained by the XENON100 non-blind analysis.

In this paper, we show that the current generation of direct detection experiments can observe a directional signal from MiDM. For concreteness we focus on a XENON100-like detector, for two reasons. First, XENON100 will soon place strong constraints on the MiDM parameter space, making it the most relevant experiment to consider. Second, we wish to emphasize the feasibility of detecting a directional signal with experiments that are currently running.

We compute the distribution of recoil track angles and velocities from MiDM benchmarks. The sensitivity of XENON100 to the MiDM parameter space depends strongly on the lifetime of the excited state. For the benchmark lifetimes of $\sim 1 - 10\mu$s, XENON100 can measure the directional modulation at high significance and obtain sharp constraints on the parameter space with just tens of events. This is achievable with around 5000 kg $\cdot$ day in the energy range $10 - 80$ keVr.

II. DIRECTIONAL DETECTION

Directional detection can clearly test whether any signal comes from WIMP interactions [43]. Due to the Earth's motion in the Galaxy, there is a "WIMP wind" which is opposite the motion of the Earth. There is a

daily modulation in the angle of recoil tracks in the lab frame. This modulation depends only on the rotation of the Earth relative to the WIMP wind, and can be disentangled from the daily rotation of the Earth with respect to the Sun. The experimental directional detection effort focuses on measuring the nuclear recoil track with large-volume, gaseous detectors [44–46].

Angular information is a particularly powerful discriminant of WIMP scattering for iDM [47, 48]. Because inelastic interactions have a high velocity threshold, the angular distribution of the nuclear recoil tracks is sharply peaked in the direction of the WIMP wind. There is a kinematic constraint on the recoil angle of the nucleus:

$$(\cos\gamma)_{max}(E_R) = \frac{v_{esc} - v_{min}(E_R,\delta)}{v_E}. \qquad (3)$$

Here γ is the angle between the velocity of the Earth and the recoil velocity in the Earth frame, v_E is the Earth's velocity in the Galactic frame, and v_{esc} is the Galactic escape velocity from the Solar neighborhood. For typical iDM models considered in the literature, γ is constrained to be within $\sim$100 degrees of the WIMP wind [47]. However, because the signal goes to zero at the bound in Eq. 3, the precise location of this kinematic constraint can be difficult to pinpoint.

MiDM has better directional detection prospects at XENON100, compared to directional detection of iDM. Current directional detectors focus on spin-dependent scattering and use light targets such as CF_4 [49–52]. Thus, they would not see inelastic scattering events. In the MiDM case, there is also much more event information and thus more sensitivity to the parameter space. One can measure both the velocity (v_*) and the angle ($\cos\gamma_*$) of the WIMP recoil track. Once again, this recoil angle is with respect to the Earth's motion. The tracks are sharply peaked in angle opposite the motion of the Earth.

For the WIMP recoil angle, there is also an energy-dependent maximum recoil angle, which we give in Sec. III. The most important bound is on the WIMP recoil velocity,

$$v_*^{min}(E_R) = \left|\frac{(E_R(m_N/m_\chi - 1) - \delta)}{\sqrt{2m_N E_R}}\right|. \qquad (4)$$

Here the signal peaks near the kinematic bound because most events occur near the threshold velocity in Eq. 1. Thus having information on both v_* and E_R is an extremely sensitive probe of the model parameters. There is a remaining degeneracy: if δ and m_χ are shifted in *opposite* directions, the bound can remain roughly the same. However, one can fit δ separately from the spectrum of the nuclear recoils, and from the energy of the emitted photons.

There is also a maximum velocity for the excited state,

$$v_*^{max}(E_R) = \sqrt{(v_E + v_{esc})^2 - 2(E_R + \delta)/m_\chi}, \qquad (5)$$

but the rate is exponentially suppressed at this bound.

A. XENON100

We model directional detection in XENON100 with a simplified XENON100-like experiment. XENON10 [24, 53] had 316.4 kg· day of data in the energy range 4.5-75 keVr. XENON100 has a 40 kg fiducial mass, at even lower backgrounds. The initial 170 kg· day non-blind run already constrains the MiDM parameter space (at low δ).

The XENON100 detector is a cylinder, with a radius of 15.3 cm and a height of 30.6 cm. The fiducial volume has a radius of 13.5 cm and height of 24.3 cm. The primary scintillation (S1) and ionization (S2) signals of an event are measured. For more details, see [54]. The S2 signal is observed 15-140 μs after the S1 signal, for events in the fiducial volume.

The signature of MiDM is two S1 signals separated by roughly .5 μs in time, followed at least 15 μs later by two S2 signals. The photon event is identified from the second S1 signal and an S2 peak with energy of $\sim$100 keVee. At 100 keVee, a photon is clearly distinguishable from a nuclear recoil by S2/S1. The other event should be consistent with a nuclear recoil. The time separation of the two S2 signals depends on how the WIMP recoils along the cylinder axis, z. In XENON10, events with multiple S2 events at different z positions were rejected.

We refer to the track connecting the two events as the decay track. Events can be localized to a 3D spatial resolution of 3 mm (though the absorption length for the 100 keV photon may blur this) and timing resolution of 10 ns. Meanwhile, the track should be at least 10 cm long. This makes it possible to measure direction and velocity of the decay track to an extremely high accuracy. The head-tail discrimination of the track can be determined using timing information and the S1/S2 ratio.

We wish to obtain the χ^* recoil track from the decay track. However, because the photon can travel up to $\sim$1 cm after emission, this introduces systematic uncertainties. The observed decay track can be blurred by a few degrees, relative to the χ^* recoil track direction. This also introduces an uncertainty in the velocity of the χ^* of roughly 10%.

There are some specific event geometries that can result in more ambiguous events. For example, it could be difficult to resolve the two S2 signals if the decay track is perpendicular to the z axis. Then the two S2 signals arrive at nearly the same time. S2 signals generally have a time width of $\sim 1\mu$s and the PMT spatial resolution is only $\sim$2.5 cm. However, because the drift velocity is 2mm/μs, this is a small fraction of the total solid angle.

Thus directional events are in principle detectable at XENON100. The background for such delayed coincidence events with both a nuclear recoil and a photon of energy $\sim$ 100 keV should be extremely low. There are other 'mixed' delayed coincidence events from Bi and Kr contamination, and excitation of metastable states of Xe [54]. However, these have very different energies and decay times. It may be possible to extend the fiducial volume when searching for directional events.

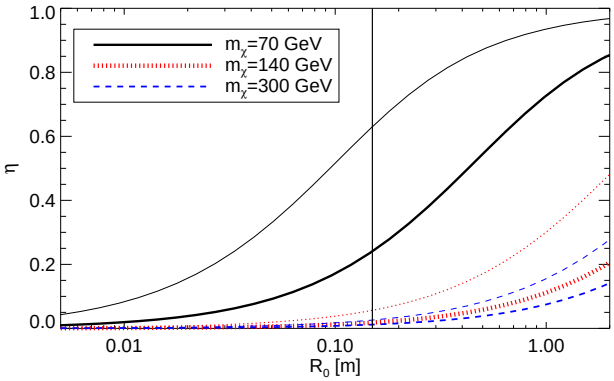

FIG. 1: The efficiency η for the best-fit benchmarks from Table I. R_0 is the size of a spherical detector. We approximate the XENON100 fiducial volume as a sphere with radius $R_0 = 0.15$ m, marked by the vertical black line. The thinner lines show the corresponding results with highest δ, within the 90% CL region of the best fit.

B. Detector Efficiency

The typical decay length is $1 - 10$ m in these models, relatively large compared to XENON100. Thus the WIMP can recoil inside the detector volume, but decay outside the detector [60]. The effective exposure for delayed coincidence events is, in general, lower than the exposure for nuclear recoils because of this geometric effect. Here we compute the detector efficiency, as a function of typical detector size, for the MiDM benchmarks.

The efficiency is

$$\eta(t) = \int d^3\vec{v}_* f(\vec{v}_*, t) \int \frac{dt'}{\tau} e^{-t'/\tau} \left(\int_V \frac{d^3\vec{x}}{V} H(t, \vec{x}, \vec{d}, t') \right)$$

The term in brackets comprises detector effects. The spatial integral is over the detector volume. $H(t, \vec{x}, \vec{d}, t')$ is the efficiency for observing a WIMP decay, given that a nuclear recoil was observed. This depends on the time of the year t, the location of the WIMP-nucleus interaction inside the detector, $\vec{x}$, the decay vector, $\vec{d}$, and the WIMP decay time (coincidence time), t'. Whether a given WIMP decay track is located inside the detector depends on the orientation of the detector with respect to the Earth's velocity, the decay vector, and the efficiency for the particular event geometry.

The astrophysics and particle physics is captured by the integral over t' and $\vec{v}_*$. τ is the lifetime of the excited state. The distribution of recoils depends on the WIMP recoil velocity distribution, $f(\vec{v}_*)$, and the decay time distribution. We assume that $\vec{v}_*$ is defined with respect to the Earth's velocity vector so that $f(\vec{v}_*)$ does not depend on detector orientation.

For the calculation below, we model the detector as a single sphere of size R_0. We assume that H depends only on the interaction position $\vec{x}$ and the decay length $L = v_* t'$. Here we neglect the smearing arising from the mean free path of the emitted photon, since the emission is isotropic. There is also no dependence on t or recoil angle in this approximation. Then the expression for efficiency above can be simplified to

$$\eta = \int dL\ g(L) \int_0^{R_0} \frac{3R^2 dR}{R_0^3} H(R, L) \tag{6}$$

where L is the recoil length. The recoil length distribution $g(L)$ is

$$g(L) = \int dv_* \frac{f(v_*)}{v_* \tau} \exp\left(-\frac{L}{v_* \tau}\right) \tag{7}$$

where now $f(v_*)$ is the distribution for v_*, not $\vec{v}_*$. A good approximation is $g(L) = \exp(-L/\lambda)/\lambda$, where $\lambda = \langle v_* \rangle \tau$ is the average recoil length. Typical λ values are given in Table I.

We approximate the XENON100 detector as a sphere. The fiducial volume has radius $R_0 = 15$ cm, with efficiency $\eta_{.15}$. Results are shown in Fig. 1. The precise efficiency depends on specifics of the detector, and must take into account the effects mentioned in Sec. II A.

III. RECOIL SPECTRUM

There are two electromagnetic scattering channels for magnetic dark matter: dipole-dipole and dipole-charge. In the dipole-dipole scattering case, the dark matter interacts with the magnetic moment of the nucleus. The matrix element is

$$\frac{|\mathcal{M}|^2}{32\pi m_N m_\chi^2} = 16\pi\alpha^2 m_N \left(\frac{\mu_{nuc}}{e}\right)^2 \left(\frac{\mu_\chi}{e}\right)^2 \frac{S_N + 1}{3S_N}, \tag{8}$$

for each isotope. We sum over all isotopes, weighted by their abundances [17]. There is, in general, also a factor of $(S_\chi + 1)/(3S_\chi)$ for the spin of the dark matter. We take $S_\chi = 1/2$.

In the dipole-charge scattering case, the dark matter interacts with the electric charge of the nucleus. The matrix element is

$$\frac{|\mathcal{M}|^2}{32\pi m_N m_\chi^2} = \frac{4\pi Z^2 \alpha^2}{E_R} \left(\frac{\mu_\chi}{e}\right)^2 \Big[v^2 - E_R \left(\frac{1}{2m_N} + \frac{1}{m_\chi}\right) - \delta \left(\frac{1}{\mu_{N\chi}} + \frac{\delta}{2m_N E_R}\right) \Big], \tag{9}$$

where v is the initial velocity of the WIMP in the lab frame. We have again assumed $S_\chi = 1/2$.

The differential scattering rate for measuring both nuclear recoil energy and WIMP recoil track is

$$\frac{dR}{dE_R dv_* dx_*} = \frac{\eta N_T \rho_\chi}{m_\chi} \int d^3\vec{v}\ f(\vec{v} + \vec{v}_E)\ v\ \frac{d\sigma}{dE_R dv_* dx_*} \tag{10}$$

where we have abbreviated $x_* = \cos\gamma_*$. The three-dimensional WIMP velocity distribution is given by $f(\vec{v})$.

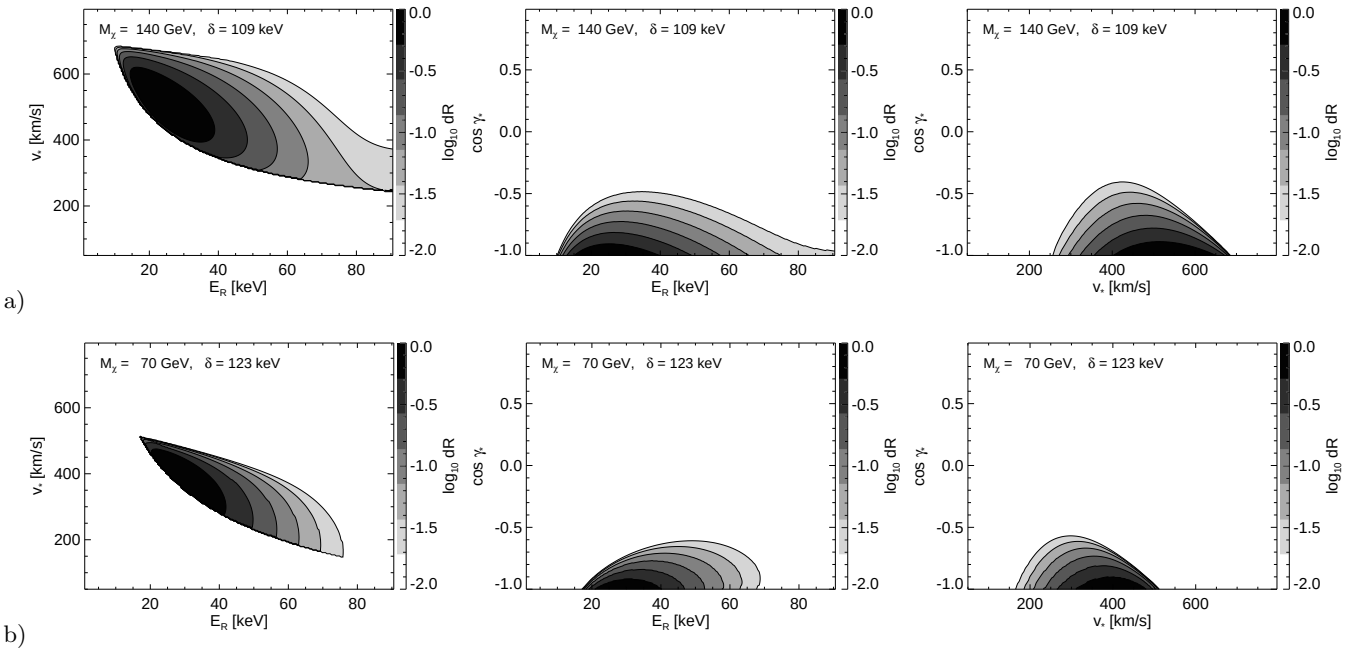

FIG. 2: Differential rates $dR/(dE_R d\cos\gamma_* dv_*)$ for (a) $m_\chi = 140$ GeV MiDM benchmark and (b) $m_\chi = 70$ GeV MiDM benchmark. The $m_\chi = 300$ GeV benchmark looks similar to the $m_\chi = 140$ GeV benchmark. In each case we show three two-dimensional distributions, where we have integrated over the third variable. All rates are computed assuming scattering on Xe, and benchmarks are given in Table I. The differential rate is normalized so that the total rate is unity.

N_T is the number of target nuclei per kg and ρ_χ is the local WIMP energy density, which we fix to be 0.4 GeV/cm^3 [55].

As in [47], we expand $d\sigma$ and change variables to $\vec{v}' = \vec{v} + \vec{v}_E$. The trivial integral over $\vec{v}'$ imposes the condition

$$\vec{v}' = \vec{q}/m_\chi + \vec{v}_* + \vec{v}_E. \tag{11}$$

$\vec{q}$ is the recoil momentum of the nucleus. The resulting differential rate is

$$dR = \frac{\eta N_T \rho_\chi}{m_\chi} d^3\vec{v}_* d^3\vec{q}\; f(\vec{v}') \left(\frac{|\mathcal{M}|^2}{64\pi^2 m_\chi^2 m_N^2}\right) F^2[E_R] \times \delta^{(1)}\left(\frac{q^2}{2m_\chi} + \vec{q}\cdot\vec{v}_* - E_R - \delta\right). \tag{12}$$

$F^2[E_R]$ is a nuclear form factor which depends on the type of interaction.

For a xenon target, dipole-charge scattering, Eq. 9, dominates. For this we use the standard nuclear Helm form factor. Dipole-dipole scattering, Eq. 8, is roughly 20% of the total rate. To calculate dipole-dipole scattering a magnetic moment form factor is necessary. The nuclear magnetic moment receives contributions from both spin and angular momentum. We use the spin form factor from [56]. The angular momentum component is $\sim 20-30\%$ at zero momentum for Xe. Since dipole-dipole scattering is already subdominant for Xe, and since we do not have accurate angular momentum form factors, we approximate the entire magnetic moment form factor with the spin component.

We now specialize to the case where $f(\vec{v})$ is a normalized, truncated Maxwell-Boltzmann distribution, with $v_{esc} = 550$ km/s [57] and $v_0 = 220$ km/s. We assume $v_E = 240$ km/s on average and label the normalization factor of the distribution as $n(v_0, v_{esc})$. The result is

$$\frac{dR}{dE_R dv_* dx_*} = \frac{\eta N_T \rho_\chi v_*}{m_\chi} \frac{|\mathcal{M}|^2}{32\pi m_N m_\chi^2} F^2[E_R]\Theta(1-|x_q|) \times \int d\phi \frac{e^{-(v')^2/v_0^2}}{n(v_0, v_{esc})}\Theta(v_{esc} - |\vec{v}'|) \tag{13}$$

with the following definitions:

$$x_q = -\frac{(E_R(m_N/m_\chi - 1) - \delta)}{q v_*}, \quad \text{and} \tag{14}$$

$$(v')^2 = v_E^2 + q^2/m_\chi^2 + v_*^2 + 2v_E v_* x_* + 2x_q v_* q/m_\chi + 2v_E q/m_\chi\left(x_q x_* + \sqrt{1-x_q^2}\sqrt{1-x_*^2}\cos\phi\right).$$

An upper bound on x_* can be extracted from setting $v' = v_{esc}$, with $\cos\phi = -1$. The bound depends on both v_* and E_R.

Finally, the matrix elements are given in Eq. 8 or in Eq. 9. Note that in the dipole-charge scattering case we need to replace v in Eq. 9 using the energy conservation relation, $m_\chi v^2 = 2E_R + m_\chi v_*^2 + 2\delta$.

The normalized total rate spectrum of several benchmark models is shown in Fig. 2.

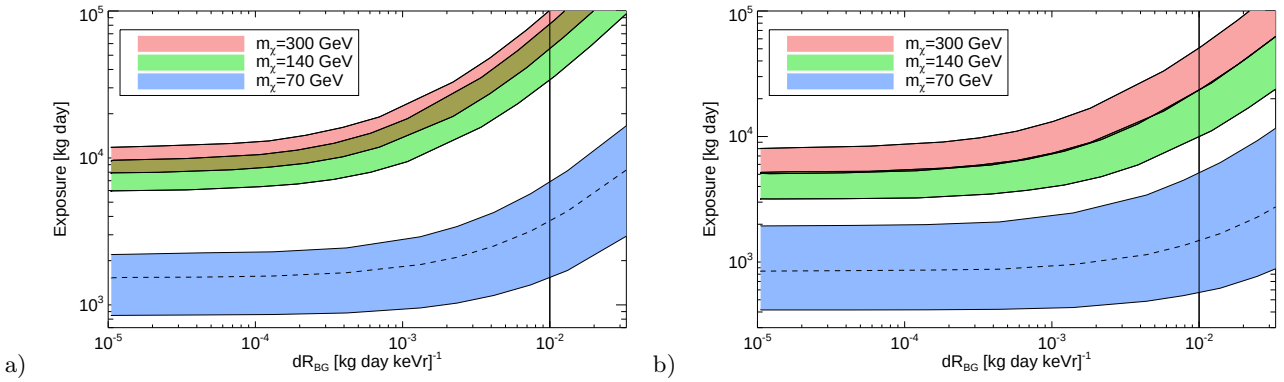

FIG. 3: Exposure to obtain a 5σ measurement of $\langle\cos\gamma_*\rangle$ 90% of the time the experiment is conducted on Earth. The energy range of the experiment is $10-80$ keVr. dR_{BG} is the background rate; a XENON maximum background rate is indicated by the solid vertical line. The bands shown give the exposures necessary as the rates modulate throughout a year. We show (a) three mass benchmarks and (b) three mass benchmarks in the 90% CL region with highest delta, from Table I.

IV. SENSITIVITY

XENON100 is collecting several thousand kg· day of exposure. We assume a total exposure of 5000 kg· day on a 40.6 kg fiducial target, in a nuclear recoil energy range of 10-80 keVr. This is consistent with scaling up the results from XENON10 and with preliminary results reported by XENON100.

For the best-fit parameters listed in Table I, this would imply a minimum of ~ 100 nuclear recoils observable by XENON100. Only ~ 10 delayed coincidence events are expected, due to the small size of the detector relative to the average recoil track length. Despite these low efficiencies, a study of the delayed coincidence events is still vastly more informative in two ways: (a) it establishes a directional signal correlated with the WIMP wind, and (b) it is much more sensitive to the parameter space.

A. Directional Detection

We first determine the exposures required to establish a correlation with the WIMP wind. The average nuclear recoil angle with respect to the Earth's motion, $\langle\cos\gamma\rangle$, is a robust model-independent statistic for directional detection [47, 58, 59]. Here we use $\langle\cos\gamma_*\rangle$, the WIMP recoil angle with respect to the Earth's motion. Because of the rotation of the Earth, on average $\langle\cos\gamma\rangle$ or $\langle\cos\gamma_*\rangle$ should be consistent with 0 for standard backgrounds.

Because XENON100 has excellent spatial resolution, we assume that the recoil track angle can be determined to 10 degrees. We compute the exposures required to obtain a 5σ result for $\langle\cos\gamma_*\rangle$ 90% of the time. We allow for a uniform (isotropic) background, though the XENON100 background should be negligibly low. The results are shown in Fig. 3. The required exposures roughly correspond to a minimum of 16 events at zero background.

B. Parameter Estimation

The predicted rate for delayed coincidence events at XENON100 is only a few counts per 1000 kg · day. However, the additional recoil track information makes it possible to obtain an excellent measurement of the model parameters.

We perform a likelihood analysis, as described in [47], over the parameter space of m_χ, δ, and μ_χ. We compute the (relative) log likelihoods for $\mathcal{E}$ kg· day on Xe, with nuclear recoil energy range $10-80$ keVr. We neglect the effects of imperfect angular and energy resolution. (The XENON100 energy resolution is $\sim 10\%$ in this energy range, and we estimate an angular resolution of 10 degrees.) The log likelihood is

$$\ln\mathcal{L}_{tot}(p) = \mathcal{E}\int dx\Big(\mu(x;p_0)\ln\mu(x;p) - \mu(x;p)\Big) \quad (15)$$

where p refers to $(m_\chi, \delta, \mu_\chi)$ and x refers generically to the event space of either E_R or $(E_R, v_*, \cos\gamma_*)$. p_0 are the true model parameters. μ is the rate for parameters p. If there is only nuclear recoil energy information,

$$\mu(E_R;p) \equiv \frac{dR}{dE_R}(E_R;p) + dR_{BG}, \quad (16)$$

in cpd/kg/keVr for parameters p. We assume the background rate, dR_{BG} is known and negligibly small.

If there is directional information,

$$\mu(E_R, v_*, x_*; p) \equiv \eta_{.15}(p)\frac{dR}{dE_R dv_* dx_*}(E_R, v_*, x_*; p) + \frac{dR_{BG}}{dv_* dx_*},$$

where $x_* = \cos\gamma_*$. $\eta_{.15}(p)$ is the efficiency, for parameters p, at XENON100.

In Fig. 4 we show the sensitivity to MiDM parameters if (1) only nuclear recoil information is used and (2) if only delayed coincidence events are considered for 5000 kg · day. We show confidence levels of (68, 90, 95, 99,

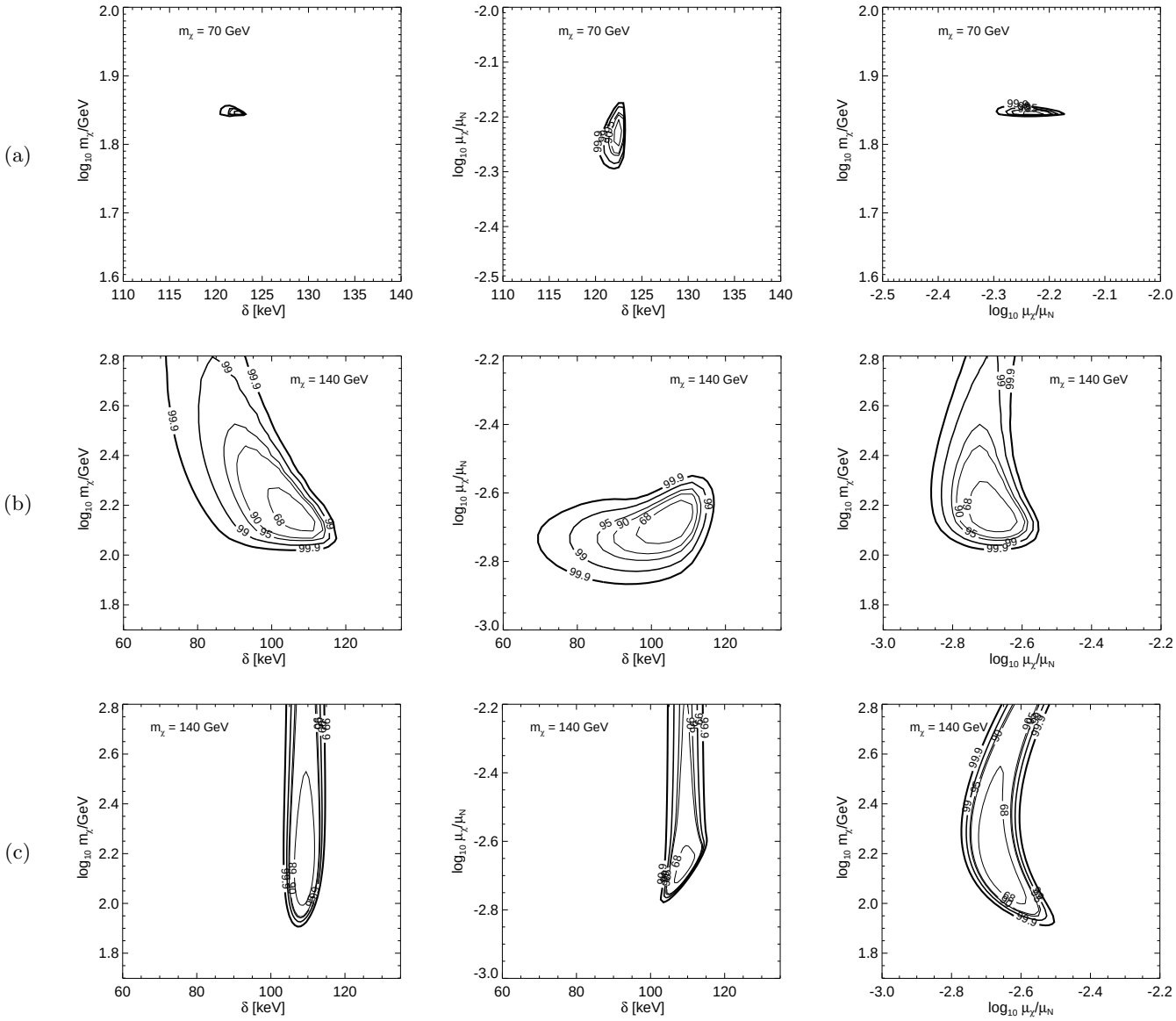

FIG. 4: Confidence levels for determining m_χ, δ, and μ_χ, marginalized over the third parameter for each two-dimensional slice. We assume an exposure of 5000 kg· day on Xe in the energy range $10-80$ keVr. The plots show sensitivity to the MiDM parameter space, using only delayed coincidence data, for the (a) $m_\chi = 70$ GeV benchmark, and (b) $m_\chi = 140$ GeV benchmark. (c) shows the sensitivity using only nuclear recoil events, for the $m_\chi = 140$ GeV benchmark. The directional information is a better test of m_χ and μ_χ. The case with $m_\chi = 300$ GeV looks similar to $m_\chi = 140$ GeV.

and 99.9%). We neglect the Earth's velocity about the Sun since a livetime of order a year is needed for 5000 kg · day.

Despite the reduction by a factor of 10-50 in events, the directional data is a much stronger constraint on m_χ and μ_χ. δ can also be determined from the E_R data or the photon energies. In Fig. 5 we show the sensitivity to m_χ and μ_χ for the $m_\chi = 140$ GeV benchmark, assuming that δ is already known. The directional information breaks the degeneracy in m_χ and μ_χ when only nuclear recoil information is used.

C. Measurement of Both Recoils

So far, we considered measurement of the WIMP recoil velocity vector from delayed coincidence events. With a gaseous directional detector, it is also possible to obtain the recoil angle of the nucleus. Then m_χ and δ are highly constrained. For such events there are 4 equations and 5 unknowns: m_χ, δ, and $\vec{v}$. However, one can obtain δ from the energy peak of the coincident photons. Then it is possible to measure the WIMP mass and velocity with just 1 WIMP scattering event. The mass is determined

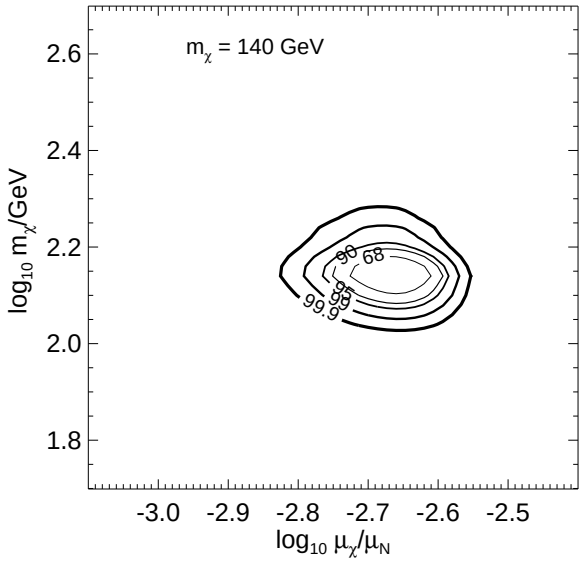

FIG. 5: Confidence levels for determining m_χ and μ_χ using WIMP recoil tracks, assuming δ is already measured from the photon energies or nuclear recoil spectrum. Here we take the $m_\chi = 140$ GeV benchmark and assume an exposure of 5000 kg· day on Xe in the energy range $10 - 80$ keVr.

by the following equation:

$$m_\chi = \frac{2m_N E_R}{2(\delta + E_R) - \sqrt{2m_N E_R}\,\hat{q}\cdot\vec{v}_*}. \qquad (17)$$

Since $\vec{q}$ and $\vec{v}_*$ are measured, the initial WIMP velocity $\vec{v}$ is then fixed by momentum conservation. A direct measurement of the WIMP velocity distribution is then also possible.

V. CONCLUSIONS

The magnetic inelastic dark matter model has an interesting and previously unstudied signature at direct detection experiments: a delayed coincident photon with energy δ. Observation of such photons would also allow current direct detection experiments to become excellent directional detectors.

Motivated by the MiDM setup, we studied several benchmark model parameters that can fit the combined DAMA/NaI and DAMA/LIBRA data. Given the rapidly improving constraints from other experiments, we feel that MiDM is currently the best hope for a dark matter interpretation of DAMA – *and it predicts a low-background signature detectable with current experiments.*

With 5000 kg· day of exposure, XENON100 can detect the angular modulation of the recoils and determine the MiDM model parameters. While we focused on benchmarks in MiDM, we emphasize that such a delayed coincidence signal is worth searching for in general. Such events, if found, carry much more information than simple nuclear recoils, and would provide more direct access to the WIMP velocity distribution in our halo.

Acknowledgments

We thank Peter Sorensen, Neal Weiner, and Itay Yavin for useful discussion. We are partially supported by NASA Theory grant NNX10AD85G. This research made use of the NASA Astrophysics Data System (ADS) and the IDL Astronomy User's Library at Goddard [61].

[1] R. J. Gaitskell, Ann. Rev. Nucl. Part. Sci. **54**, 315 (2004).
[2] R. Bernabei et al. (DAMA), Phys. Lett. **B480**, 23 (2000).
[3] R. Bernabei et al. (DAMA), Eur. Phys. J. **C56**, 333 (2008), 0804.2741.
[4] R. Bernabei et al., Eur. Phys. J. **C67**, 39 (2010), 1002.1028.
[5] R. Bernabei et al., Eur. Phys. J. **C53**, 205 (2008), 0710.0288.
[6] M. Fairbairn and T. Schwetz, JCAP **0901**, 037 (2009), 0808.0704.
[7] C. Savage, G. Gelmini, P. Gondolo, and K. Freese, JCAP **0904**, 010 (2009), 0808.3607.
[8] P. Ullio, M. Kamionkowski, and P. Vogel, JHEP **07**, 044 (2001), hep-ph/0010036.
[9] B. Feldstein, A. L. Fitzpatrick, and E. Katz, JCAP **1001**, 020 (2010), 0908.2991.
[10] Y. Bai and P. J. Fox, JHEP **11**, 052 (2009), 0909.2900.
[11] R. Foot, Phys. Rev. **D78**, 043529 (2008), 0804.4518.
[12] S. Chang, A. Pierce, and N. Weiner, JCAP **1001**, 006 (2010), arXiv:0908.3192.
[13] S. Chang, J. Liu, A. Pierce, N. Weiner, and I. Yavin, JCAP **1008**, 018 (2010), 1004.0697.
[14] S. Chang, N. Weiner, and I. Yavin, Phys.Rev. **D82**, 125011 (2010), 1007.4200.
[15] J. Bagnasco, M. Dine, and S. D. Thomas, Phys. Lett. **B320**, 99 (1994), hep-ph/9310290.
[16] M. Pospelov and T. ter Veldhuis, Phys. Lett. **B480**, 181 (2000), hep-ph/0003010.
[17] T. Banks, J.-F. Fortin, and S. Thomas (2010), 1007.5515.
[18] W. S. Cho, J.-H. Huh, I.-W. Kim, J. E. Kim, and B. Kyae, Phys. Lett. **B687**, 6 (2010), 1001.0579.
[19] V. Barger, W.-Y. Keung, and D. Marfatia, Phys.Lett. **B696**, 74 (2011), 1007.4345.
[20] A. Fitzpatrick and K. M. Zurek, Phys.Rev. **D82**, 075004 (2010), 1007.5325.
[21] E. Masso, S. Mohanty, and S. Rao, Phys. Rev. **D80**, 036009 (2009), 0906.1979.
[22] H. An, S.-L. Chen, R. N. Mohapatra, S. Nussinov, and Y. Zhang, Phys. Rev. **D82**, 023533 (2010), 1004.3296.
[23] Z. Ahmed et al. (The CDMS-II), Science **327**, 1619

(2010), 0912.3592.
[24] J. Angle et al. (XENON10), Phys. Rev. **D80**, 115005 (2009), 0910.3698.
[25] E. Aprile et al. (XENON100), Phys. Rev. Lett. **105**, 131302 (2010), 1005.0380.
[26] S. Chang, G. D. Kribs, D. Tucker-Smith, and N. Weiner, Phys.Rev. **D79**, 043513 (2009), 0807.2250.
[27] K. Schmidt-Hoberg and M. W. Winkler, JCAP **0909**, 010 (2009), 0907.3940.
[28] W. Seidel, for CRESST-II (2010), presented at Identification of Dark Matter, Montpellier, France.
[29] D. Y. Akimov et al. (ZEPLIN-III), Phys. Lett. **B692**, 180 (2010), 1003.5626.
[30] J. Kopp, T. Schwetz, and J. Zupan, JCAP **1002**, 014 (2010), 0912.4264.
[31] K. Sigurdson, M. Doran, A. Kurylov, R. R. Caldwell, and M. Kamionkowski, Phys. Rev. **D70**, 083501 (2004), astro-ph/0406355.
[32] S. Gardner, Phys. Rev. **D79**, 055007 (2009), 0811.0967.
[33] J. Goodman et al., Nucl. Phys. **B844**, 55 (2011), 1009.0008.
[34] B. Feldstein, P. W. Graham, and S. Rajendran, Phys.Rev. **D82**, 075019 (2010), 1008.1988.
[35] B. Holdom, Phys.Lett. **B178**, 65 (1986).
[36] M. Pospelov, A. Ritz, and M. B. Voloshin (2007), arXiv:0711.4866 [hep-ph].
[37] S. K. Kim (KIMS), J. Phys. Conf. Ser. **120**, 042021 (2008).
[38] J. March-Russell, C. McCabe, and M. McCullough, JHEP **0905**, 071 (2009), * Brief entry *, 0812.1931.
[39] M. Kuhlen et al., JCAP **1002**, 030 (2010), 0912.2358.
[40] F. S. Ling, E. Nezri, E. Athanassoula, and R. Teyssier, JCAP **1002**, 012 (2010), 0909.2028.
[41] M. Vogelsberger, A. Helmi, V. Springel, S. D. White, J. Wang, et al. (2008), * Brief entry *, 0812.0362.
[42] D. S. M. Alves, M. Lisanti, and J. G. Wacker, Phys. Rev. **D82**, 031901 (2010), 1005.5421.
[43] D. N. Spergel, Phys. Rev. **D37**, 1353 (1988).
[44] S. Ahlen, N. Afshordi, J. Battat, J. Billard, N. Bozorgnia, et al., Int.J.Mod.Phys. **A25**, 1 (2010), * Brief entry *, 0911.0323.
[45] G. Sciolla, Mod.Phys.Lett. **A24**, 1793 (2009), * Brief entry *, 0811.2764.
[46] G. Sciolla and C. Martoff, New J.Phys. **11**, 105018 (2009), * Brief entry *, 0905.3675.
[47] D. P. Finkbeiner, T. Lin, and N. Weiner, Phys. Rev. **D80**, 115008 (2009), 0906.0002.
[48] M. Lisanti and J. G. Wacker, Phys. Rev. **D81**, 096005 (2010), 0911.1997.
[49] E. Daw et al. (2010), 1010.3027.
[50] K. Miuchi et al., Phys. Lett. **B654**, 58 (2007), 0708.2579.
[51] S. Ahlen, J. Battat, T. Caldwell, C. Deaconu, D. Dujmic, et al., Phys.Lett. **B695**, 124 (2011), 1006.2928.
[52] C. Grignon, J. Billard, F. Mayet, and D. Santos (2010), 1008.4712.
[53] J. Angle et al. (XENON10), Phys. Rev. Lett. **100**, 021303 (2008), 0706.0039.
[54] E. Aprile et al. (XENON Collaboration), Astropart.Phys. **34**, 679 (2011), 1001.2834.
[55] R. Catena and P. Ullio (2009), 0907.0018.
[56] M. T. Ressell and D. J. Dean, Phys. Rev. **C56**, 535 (1997), hep-ph/9702290.
[57] M. C. Smith et al., Mon. Not. Roy. Astron. Soc. **379**, 755 (2007), astro-ph/0611671.
[58] B. Morgan, A. M. Green, and N. J. C. Spooner, Phys. Rev. **D71**, 103507 (2005), astro-ph/0408047.
[59] A. M. Green and B. Morgan, Astropart. Phys. **27**, 142 (2007), astro-ph/0609115.
[60] The reverse can also happen, similar to the idea in [34]. The rate depends on whether the material within ∼10m of the Xe detector mostly consists of light or heavy nuclei. Aside from a 20cm layer of lead, the shielding for XENON100 consists of polyethylene, water, and copper.
[61] Available at `http://idlastro.gsfc.nasa.gov`